Field Measurement Results of the 15 T Nb_3Sn Dipole Demonstrator MDPCT1b

J. DiMarco, M. Baldini, E. Barzi, *Senior Member, IEEE*, V.V. Kashikhin, I. Novitski, T. Strauss, M. Tartaglia, G. V. Velev, A.V. Zlobin

***Abstract*—A 15 T Nb_3Sn dipole, MDPCT1, with cos-theta-type coils was developed to demonstrate a possible magnet design for a post-LHC proton-proton Collider. The magnet has 4-layer coils with 60-mm aperture, and has graded current density between the inner and outer layers to maximize performance. The coils are constrained by vertically-split, thick iron laminations, connected by aluminum I-clamps, and a thick stainless-steel skin. The magnet was previously tested at Fermilab with reduced pre-load, and achieved record 14.1 T fields at 4.5 K. Now the magnet was reassembled with full pre-load and cryogenically retested. This paper reports the magnetic measurements results of these tests, including field strength, geometrical harmonics, coil magnetization, and iron saturation characteristics of the demonstrator.**

***Index Terms*—Accelerator magnets, electromagnetic measurements, superconducting magnets.**

I. Introduction

FERMILAB, in collaboration with other members of the U.S. Magnet Development Program (US-MDP), has fabricated a 15 T Nb_3Sn dipole demonstrator suitable for a post-LHC hadron collider [1]. The magnet, MDPCT1, is based on an optimized cos-theta coil design and was first tested in 2019 at Fermilab's Vertical Magnet Test Facility (VMTF) [1]-[3]. The magnet has since been reassembled with additional coil shims shown in Fig. 1 to bring it to full preload. Now designated MDPCT1b, it has been recently tested in this new configuration with a focus on study of magnet quench performance and changes in field quality.

The MDPCT1 design has 60 mm aperture and 4-layer shell-type graded coils. Details of magnet design, fabrication and performance in the first build have been reported previously [1]. The details of MDPCT1b re-assembly and quench performance test are reported in paper [4] at this conference. Here we present the results of the MDPCT1b magnetic measurements, including dipole strength, geometrical field harmonics, and magnetization and yoke saturation effects, emphasizing field changes with respect to the original build [5]. Moreover, results from measurements of normal sextupole decay during simulated injection porch studies are also presented.

This work is supported by Fermi Research Alliance, LLC, under contract No. DE-AC02-07CH11359 with the U.S. Department of Energy, Office of Science, Office of High Energy Physics.

The authors are with Fermi National Accelerator Laboratory, P.O. Box 500, Batavia, IL 60510, USA, (e-mail: dimarco@fnal.gov).

Color versions of one or more of the figures in this paper are available online at http://ieeexplore.ieee.org.

Digital Object Identifier will be inserted here upon acceptance.

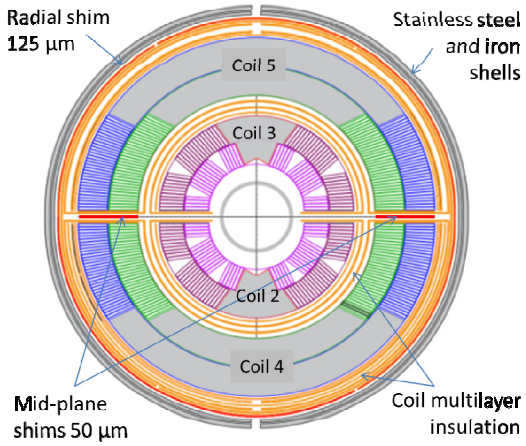

Fig. 1. MDPCT1b cross-section showing the locations of the shims added to the original build: 50 μm mid-plane shims between outer coils (coils 4 and 5), and 125 μm radial shims in all quadrants.

II. Field Definition and Measurement System

The measured field of a dipole is expressed in a standard form of harmonic coefficients defined in a series expansion of a complex field function

$$B_y + iB_x = B_1 10^{-4} \sum_{n=1}^{\infty} (b_n + ia_n) \left(\frac{x+iy}{R_{ref}}\right)^{n-1} \qquad (1)$$

where B_x and B_y are the field components in Cartesian coordinates, b_n and a_n are the normal and skew coefficients at reference radius R_{ref}, normalized to the main field, B_1, and scaled by a factor 10^4 so as to report the harmonics in convenient 'units'. For better comparison, all measurements utilize R_{ref} of 17 mm, which is the nominal value for the LHC dipole magnets. The right-handed measurement coordinate system is defined with the z-axis at the center of the magnet aperture and pointing from return to lead end, with z=0 at magnet center.

The rotating coil technique is used to measure field components. Two inductive pick-up coil probes have been fabricated using printed circuit board (PCB) technology [6]. The patterns of the radially mounted PCB have 13-turn loops on each of 16 layers. The two probe patterns on the single PCB have maximum turn area of 26 mm long ,10 mm wide and 22.7 mm integrated length ("26 mm probe"), and 130 mm long, 10 mm wide and 126.8 mm integrated length ("130 mm probe") respectively. The latter probe length approximately corresponds to one transposition pitch of the cables. Each probe has a dipole bucked signal to increase measurement accuracy of harmonics. The probe radius was constrained to be 14 mm by the

anti-cryostat diameter used for measurement, which is about 20% less than the reference radius R_{ref}.

The integration component of the data acquisition system is based on Analog-to-Digital Converter (ADC) and digital signal processor technology [7]. The system can digitize simultaneously up to 6 channels measuring the magnetic field plus the current signal, tolerating a high rotational probe speed. To mitigate the noise from the mechanical vibrations and to record the voltages from the strong dipole field, a probe speed of 0.67 Hz was used. At this speed, the combined probe and DAQ sensitivity results in signal size giving estimated resolution of about 0.1 units for a_n and b_n harmonics up to n=7.

Currents in the magnetic measurements were limited to 9 kA to avoid the possibility of additional magnet quenches.

III. Measurement Results and Discussion

A. Magnet Transfer Function

Fig. 2 shows the measured Transfer Function (TF), defined as TF≡B_1/I, of MDPCT1b versus the magnet current overlayed with the original MDPCT1 result. The TF measurement in both tests was done using the 26 mm probe to calculate magnet strength at high field [5]. Since the TF's of the two builds closely overlay, determination of the MDPCT1b field strength achieved at a given quench current followed the same extrapolation as for MDPCT1, within the 0.2% TF difference observed. The differences in TF at low and high fields between MDPCT1b and MDPCT1 suggest slightly different iron contribution in the two.

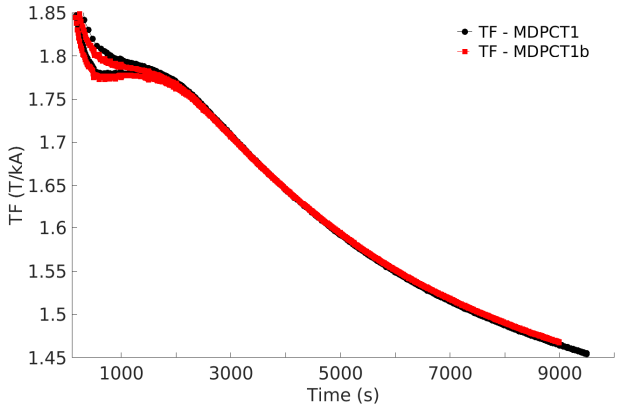

Fig. 2. Measured dipole TF versus current for MDPCT1b compared to MDPCT1 with the 26 mm probe. A small negative offset is seen for MDPCT1b at low fields and a small positive difference at high field.

Fig. 3 shows axial variation of TF at 9 kA, measured using the short rotating coil probe. As noted in [5], the observed increase of TF in the coil ends relative to z-center is consistent with the 3D COMSOL simulation [8]. Based on measurements, the non-lead 'half' is slightly stronger by about 15-20 units whereas the lead-end 'half' did not change. Since the coil shims were the same along the magnet, the observed different impact of the coil shims on the TF in the lead and non-lead ends needs to be understood. The TF across the magnet–at a current of 9000 A is ~0.1% higher on average in MDPCT1b than in the original build. Only a few unit increase in TF is expected due to geometrical coil compression with the shims. However, a field simulation with 125 μm radial shim shows that because of iron saturation effects, the TF should be 0.17% higher at 8 kA than when no shim was present.

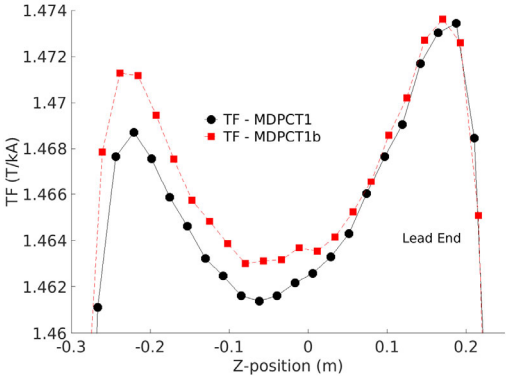

Fig. 3. Measured dipole TF at 9 kA versus magnet Z-position for MDPCT1b compared to MDPCT1 with the 26 mm probe. The MDPCT1b TF is larger for the non-lead end half, but is about the same at the lead end.

B. Low-order Field Harmonics

A comparison of the low-order normal (b_2, b_3) and skew (a_2, a_3) harmonics versus current for the two builds is shown in Fig. 4. There is generally very good consistency between the magnet builds, with no large changes from added shims except for a_3, which shows the largest change in hysteresis character, and b_3 and a_2, which also show some shifts. Perhaps coil asymmetry, which likely generates discrepancy between dipole and sextupole field directions, has gotten slightly worse after the shimming.

Fig. 5 shows axial low-order normal and skew harmonics. The harmonics are generally small being less than ±5 units in the magnet straight section (±0.3 m), except for b_3 (15 units at 9 kA), and have not changed much with the rebuild, except for a_3, which shows a 2-3 unit shift. There are also some differences at the lead end of the skew harmonics. The allowed 10-pole, b_5, along with a_4, a_5, show periodic variation on the order of 1 unit, from the effects of cable transposition pitch.

C. Decay and Snapback

To study decay and snapback during a simulated injection current, measurements were made during the current cycle shown in Fig. 6, with data taken by both 130 mm and 26 mm probes, which sample at different z-positions (the probe centers separated by 130 mm). Before this current profile, the 130 mm probe was positioned at z=0 cm, and a pre-cycle ramped the magnet to 9000 A and held for 5 minutes before returning to a holding current of 100 A to achieve a reproducible magnetization state. The harmonics decay was measured for 30 minutes upon reaching the simulated injection porch at 1100 A, and continued through snapback as upramp current ramping resumed. Similar measurements were made on the 'back porch' as the current ramped down after its cycle to 9000 A. After this first cycle, when the current was back at 100 A, the probe positions were shifted by 6 cm downward (half a cable transposition pitch), and the simulated injection cycle repeated.

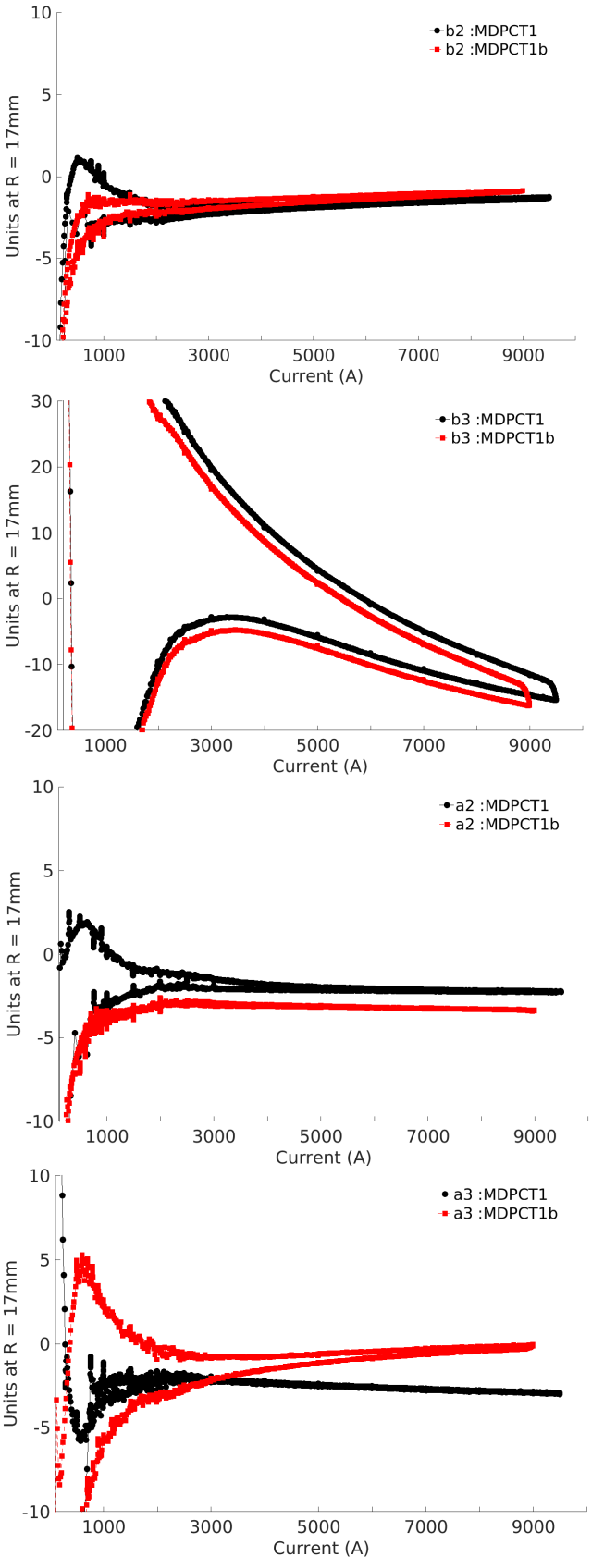

Fig. 4. Low-order normal (b_n) and skew (a_n) coefficients vs current I for MDPCT1 (black) and MDPCT1b (red).

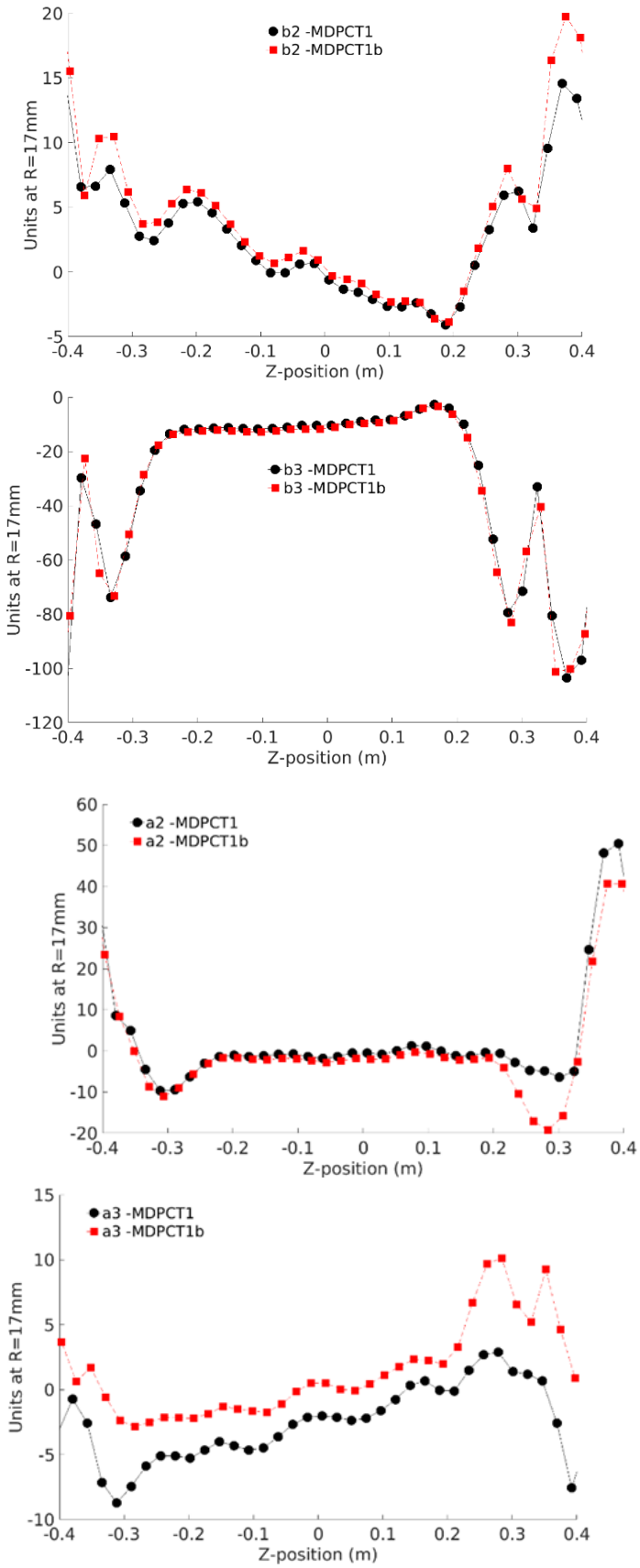

Fig. 5. Low-order normal (b_n) and skew (a_n) coefficients vs Z at 9 kA for MDPCT1 (black) and MDPCT1b (red).

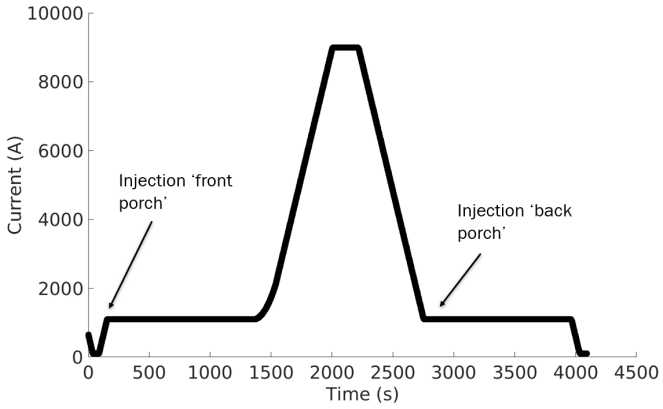

Fig. 6. Current profile used for accelerator cycle simulation during which decay and snapback measurements were made.

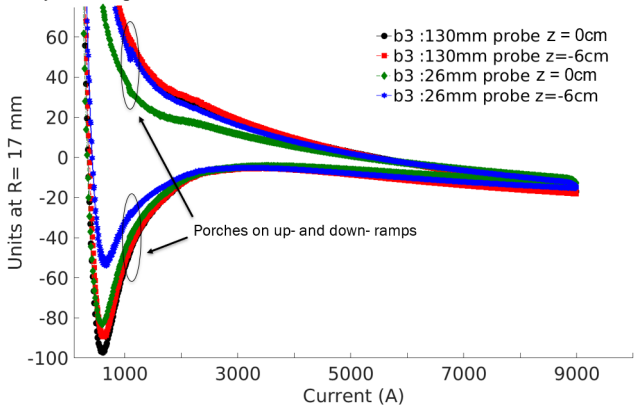

Fig. 7. b_3 hysteresis with injection 'porches' during accelerator profile.

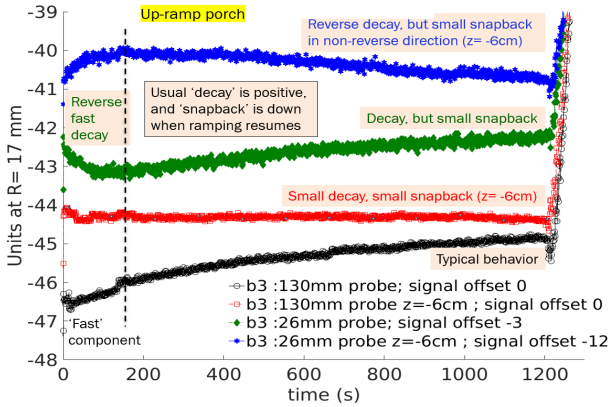

Fig. 8. b_3 decay and snapback on the 'front' porch during up-ramp to 1100 A.

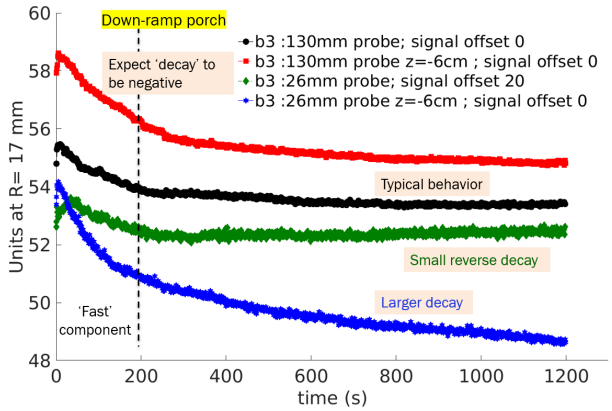

Fig. 9. b_3 decay and snapback on 'back' porch during down-ramp to 1100 A.

The b_3 hysteresis cycle during the accelerator profile is shown in Fig. 7. Results of the decay and snapback measurements are shown in Figs. 8 and 9 for the up-ramp and down-ramp porches respectively. The data were offset for clarity as noted in the legends. The 130-mm probe data seems to be fairly stable with regards to the -6 cm shift in Z-position. The up-ramp decay became more flat, indicating some dependence on position (or perhaps the effect of the small mismatch between the 11 cm cable transposition pitch and the 13 cm probe length), while the down-ramp decay seems very similar.

The 26 cm probe, which is more sensitive to the transposition pitch, shows more interesting changes. First, the decay reversed between porches on the up-ramp and down-ramp for both initial and shifted positions (i.e. between Fig. 8 and Fig. 9), and then there are reversals at some level when the probe position was changed at each of the porches (i.e. within both Fig. 8 and Fig. 9). This sensitivity is consistent with the fact that decay is related to the Boundary Induced Coupling Currents (BICC) that also create periodicity in the harmonics with respect to Z-position [9], which is evident, e.g., in Fig. 5.

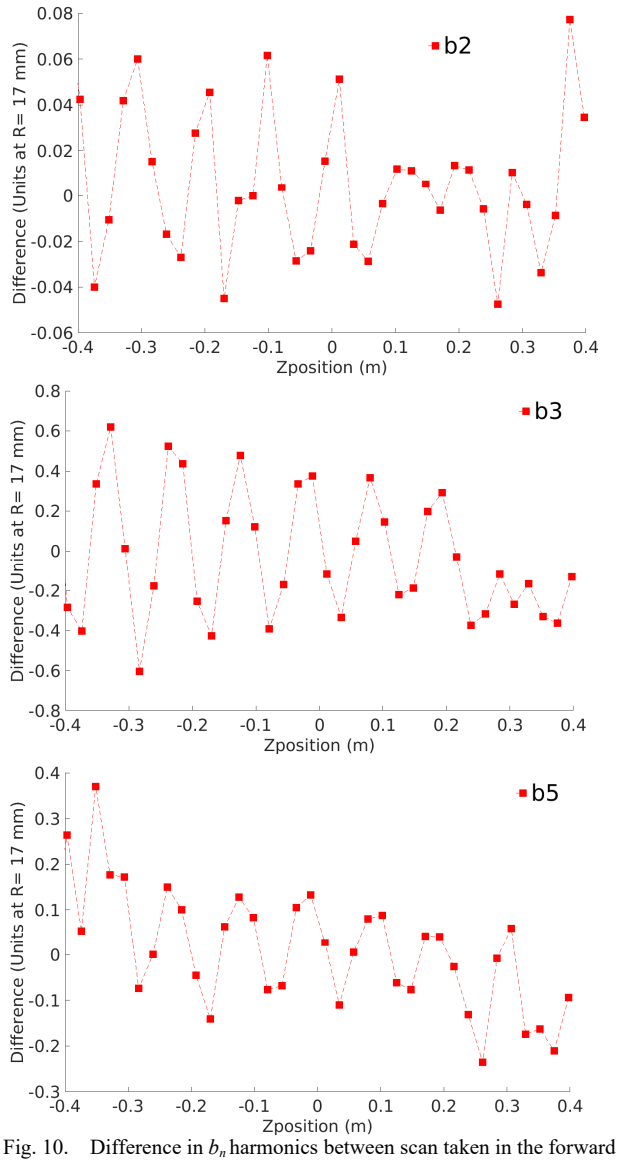

Fig. 10. Difference in b_n harmonics between scan taken in the forward Z-direction, followed by a scan taken moving in the reverse Z-direction.

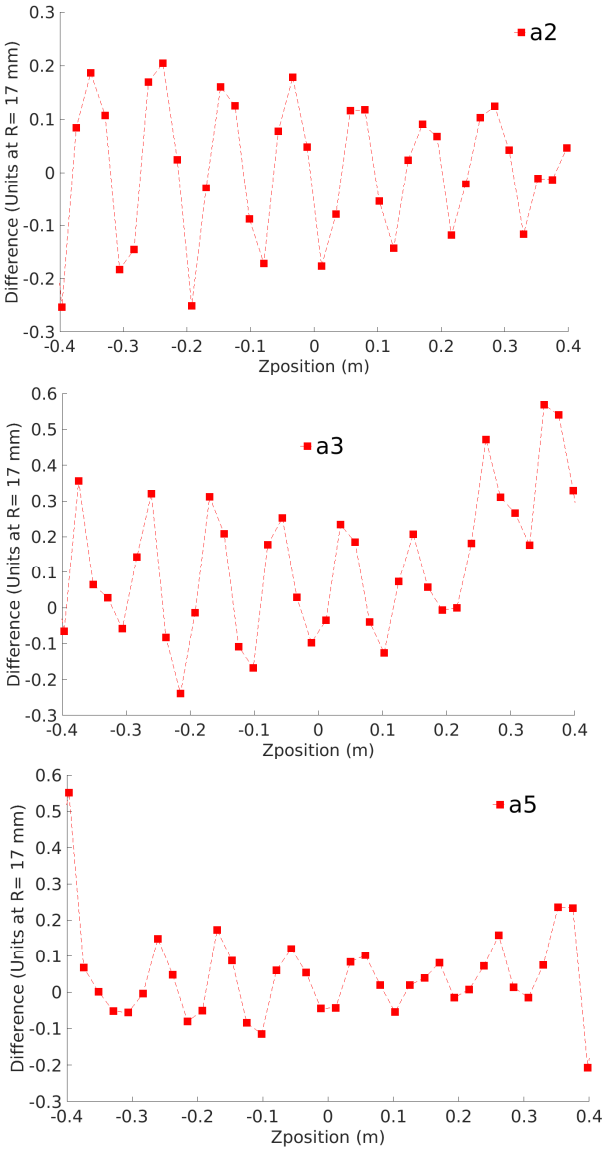

Fig. 11. Difference in a_n harmonics between scan taken in the forward Z-direction, followed by a scan taken moving in the reverse Z-direction.

To further look at the decay of the BICC, axial scans were performed in a forward direction (from -0.6 m to +0.6 m), followed by scans taken by moving in the reverse direction axially, i.e. from +0.6 m to -0.6 m at 9 kA. The results of the difference between forward and reverse scans are shown in Figs. 10 and 11. No difference would be expected if there were no time-dependent effects present, but instead clear periodic patterns are seen in all the harmonics. This demonstrates that the periodicity is related not just to transposition pitch, but also to change in time: presumably as the BICC decay in the intervening delay between Z-scan samples at a given position. The measurements were repeated at 5 kA, and similar effects seen, but with reduced amplitude.

IV. Conclusion

The dipole field strength and field harmonics for the rebuilt 15 T dipole demonstrator MDPCT1b recently tested at Fermilab are presented. The average magnet transfer function has increased by ~0.1% due to magnet coil shimming. The observed different impact of the coil shims on the TF in the lead and non-lead ends still needs to be understood. Geometrical harmonics are basically the same except for some small changes in normal and skew sextupole and other small changes at the lead end. Some harmonics (b_2, a_4) also show change between lead-end and non-lead-end halves similar to that seen in the TF. We hope to learn more about the causes of some of the subtle changes in harmonics during the disassembly and inspection of the magnet.

In the study of decay and snapback of the normal sextupole b_3, we found that local variations in measurement position of a non-transposition-pitch-integral (short) probe can cause substantially different decay profiles. We also observed that the periodic pattern associated with twist pitch changes in time for all low-order harmonics (between forward and reverse z-scans in our measurements), suggesting, therefore, that both the local variation and change in time effects are related to current re-distribution in the cable.

Acknowledgment

The authors thank the technical staff of Fermilab's Applied Physics and Superconducting Technology Division for their contribution to the magnet testing.

References

[1] A.V. Zlobin *et al*., "Development and First Test of the 15 T Nb_3Sn Dipole Demonstrator MDPCT1," in *IEEE Trans. Appl. Supercond.*, vol. 30, no. 4, June 2020, Art no. 4000805, doi: 10.1109/TASC.2020.2967686.

[2] A. V. Zlobin et al., " Design concept and parameters of a 15 T Nb3Sn dipole demonstrator for a 100 TeV hadron collider ", *Proc. IPAC*, pp. 3365-3367, May 2015.

[3] I. Novitski et al., "Development of a 15 T Nb_3Sn Accelerator Dipole Demonstrator at Fermilab," *IEEE Trans. Appl. Supercond*., vol. 26, no. 3, June 2016, Art. no. 4001007.

[4] A.V. Zlobin et. Al, "Reassembly and Test of High-Field Nb_3Sn Dipole Demonstrator MDPCT1," *IEEE Trans. Appl. Supercond., accepted for publication*.

[5] T. Strauss et al., "First Field Measurements of the 15 T Nb_3Sn Dipole Demonstrator MDPCT1," *IEEE Trans. Appl. Supercond*, vol. 30, no. 4, June 2020, Art no. 4001106, doi: 10.1109/TASC.2020.2970621.

[6] J. DiMarco et al., "Application of PCB and FDM Technologies to Magnetic Measurement Probe System Development," *IEEE Trans. Appl. Supercond*., vol. 23, no. 3, 2013, Art. no. 9000505.

[7] G.V. Velev et al., "A Fast Continuous Magnetic Field Measurement System Based on Digital Signal Processors," *IEEE Trans. Appl. Supercond*, vol. 16, no. 2, June 2006, pp. 1374-1377.

[8] COMSOL Multiphysics, https://www.comsol.com.

[9] G. Velev, et al., "Summary of the Persistent Current Effect Measurements in Nb_3Sn and NbTi Accelerator Magnets at Fermilab," *IEEE Trans. Appl. Supercond*., vol. 26, no. 4, 2016, Art. no. 4000605.